Journal of Nuclear Materials 393 (2009) 292–299

Contents lists available at ScienceDirect

Journal of Nuclear Materials

journal homepage: www.elsevier.com/locate/jnucmat

Implementing first principles calculations of defect migration in a fuel performance code for UN simulations

E.A. Kotomin [a], Yu.A. Mastrikov [a], S.N. Rashkeev [b], P. Van Uffelen [c,*]

[a] Institute for Solid State Physics, University of Latvia, 8 Kengaraga str., LV-1063 Riga, Latvia
[b] Center for Advanced Modeling and Simulation, Idaho National Laboratory, P.O. Box 1625, Idaho Falls, ID 83415-2208, USA
[c] European Commission, Joint Research Centre, Institute for Transuranium Elements, Hermann–von-Helmholtz-Platz 1, D-76344 Eggenstein-Leopoldshafen, Germany

ARTICLE INFO

Article history:
Received 15 December 2008
Accepted 16 June 2009

ABSTRACT

Results are reported of first principles VASP supercell calculations of basic defect migration in UN nuclear fuels. The collinear interstitialcy mechanism of N migration is predicted to be energetically more favourable than direct [0 0 1] hops. It is also found that U and N vacancies have close migration energies, and O impurities accelerate migration of N vacancies nearby. These values are both in qualitative agreement with the effect of oxygen on the reduction of the activation energy for thermal creep reported in the literature, as well as in quantitative agreement with the experimental data when taking into account the uncertainties. The migration energies have been implemented in the thermal creep model of the TRANSURANUS fuel performance code. Therefore a concrete example is provided of how first principles computations can contribute directly to improve the design tools of advanced nuclear fuels, e.g. the predictions reveal a limited effect of oxygen on the thermo-mechanical performance of nitride fuels under fast breeder reactor (FBR) normal operating conditions.

1. Introduction

Uranium nitrides and carbides are of considerable interest as advanced nuclear fuels and targets for fast reactors and for transmutation of Pu and minor actinides [1]. However, unlike UO_2 commercial fuels, reliable experimental data on intrinsic defect migration energies that impact fuel performance during its operation and subsequent long term storage are very scarce. In particular, the effect of oxygen impurities - unavoidable in nitrides and carbides - on intrinsic defect migration is not systematically studied, even though thermodynamic parameters have been computed for the U–Pu–N system [2].

In the last recent review of material properties for nitride fuels by Hayes et al. [3] two sets of experimental data for thermal creep are reported. Although the Arrhenius activation energy is provided, the spread of experimental data for nitride fuels with varying degree of oxygen impurities is not elucidated. More precisely, the experimental indication that oxygen impurities reduce thermal creep in UN [4] is not addressed.

With the advent of more sophisticated simulation techniques, improved hardware as well as the regained interest for fast reactor fuels for the next generation of reactors the number of theoretical studies on advanced nuclear fuels have increased (e.g. [2,5]) mainly because they constitute a cheap complement to the experiments in terms of time and resources. In line with this, a series of density functional theory (DFT) plane-wave calculations were performed for pure and defective UN [6–10]. Some studies [6,7] analysed in detail the role of basis sets (linear combination of atomic orbitals versus plane-waves) as well as how a choice of the exchange–correlation functional and inclusion of spin–orbital coupling affect the basic properties of bulk materials. A few papers only [8–10] focused on the static properties of basic radiation defects (e.g. Frenkel and Schottky pairs, vacancies) and O impurities. Furthermore, no attempts have been made so far to link first principles calculations with a macroscopic model, which is necessary for simulating the performance of a nuclear fuel pin under operational and prolonged storage conditions. In the first part of the present paper, the first principles theoretical study is extended to the intrinsic *defect migration* properties in pure and O containing UN in order to try to understand the above mentioned experimental observation. The analysis relies on the link between creep and diffusion, as highlighted by Philibert [11] for oxides and carbides. In the second part of the paper the results of these calculations are used to illustrate how sophisticated simulation tools can contribute to extend the current fuel performance codes for the prediction of advanced fuels, on the basis of an example for a UN fuel rod using the TRANSURANUS code.

2. Method

The DFT computer code VASP 4.6 [12] is employed in conjunction with the projector augmented-wave (PAW) method and the

* Corresponding author.
E-mail address: Paul.Van-Uffelen@ec.europa.eu (P. Van Uffelen).

0022-3115/$ - see front matter © 2009 Elsevier B.V. All rights reserved.
doi:10.1016/j.jnucmat.2009.06.016

plane-wave basis set. In addition, the Perdew–Wang-91 generalized gradient approximation (GGA) non-local exchange–correlation functional [13] was used together with the relativistic PAW pseudopotentials, representing the core U electrons (with $6s^2 6p^6 6d^2 5f^2 7s^2$ valence shell), N ($2s^2 2p^3$) and O ($2s^2 2p^4$) atoms (containing 14, 5 and 6 valence electrons, respectively). The plane-wave cut-off energy is chosen to be 520 eV, which is sufficient for good convergence of basic bulk properties.

The effective atomic charges were calculated using the Bader topological analysis [14]. For the defective UN rock-salt *fcc* structures three types of supercells having a different size have been used, obtained by expanding the translation vectors of the primitive cell by $3 \times 3 \times 3$ (54 atoms) [U and N vacancies, V_U and V_N, as well as O substitutional impurity], $4 \times 4 \times 4$ (128 atoms) [for studying the U-Frenkel pair and the interstitial N and U atom migration], and $5 \times 5 \times 5$ (250 atoms) [for analysing Schottky pairs]. These supercells correspond to defect concentrations of 3.7%, 1.6% and 0.8%, respectively. In these supercell calculations the standard Monkhorst–Pack scheme [15] for the $3 \times 3 \times 3$ *k*-point mesh in the Brillouin zone was applied.

Finally, to simulate a realistic process of Frenkel pair formation in the U-sublattice, a U atom was moved in a 128-atom supercell from a regular site into the interstitial position in the cube centre, at a distance of 8.6 Å from the vacancy. Complete optimisations of both the local atomic structure and the lattice constant have been performed. More details of the calculation method are provided in Ref. [8]).

Radiation produces Frenkel defect pairs (vacancies and interstitials) whose migration considerably affects material properties of the solid. In our 54-atom supercell calculations, the U and N vacancies were modelled by removing neutral atoms from their sites and allowing the rest of the ions to relax. Also 250-atom supercell calculations, containing *a pair* of well separated N and U vacancies, were carried out. The reason behind performing these two types of calculations is twofold: (i) to estimate the effects of both the supercell size and the stoichiometry, (ii) to estimate the interaction between the two defects caused by the lattice deformations and the charge density redistribution. Indeed, despite the fact that UN is a metal, the Debye screening length therein could be comparable with the distance between defects.

The saddle point of the defect migration by the vacancy mechanism corresponds to the U or N atomic position at the face centre, corresponding to the half-distance between the two adjacent sites along the [1 1 0] direction.

3. Main results

3.1. U and N vacancy migration

The main results for basic vacancy calculations with the host atom in the equilibrium and saddle point positions are summarized in Table 1. In line with recent results [8], the formation energies for these defects are close, of the order of 10 eV. The lattice energy gain due to surrounding ion relaxation is about 0.7–1.0 eV. In the equilibrium position, ionic relaxation around defects is observed within several spheres of surrounding ions. The nearest neighbour (NN) ions are displaced inward from a vacancy by 0.05 Å for the V_N and outward by 0.14 Å for the V_U, respectively. The results for the NN displacements agree with displacements found for the two individual vacancies in a 54-atom supercell (square brackets in Table 1) [8].

The ion relaxation is accompanied by the local charge redistribution. For V_N practically a whole charge of a missing N atom (−1.6 e) is localized on six NN U ions. In the case of V_U the charge perturbation area is essentially larger.

Table 1
Atomic displacements d (in Å) and change of atomic charges Δq (in e) due to a vacancy, with respect to those in relevant defect-free supercells (a) for the host ion in equilibrium and (b) for the saddle point (during diffusion). The positions are calculated using 250-atom supercells and 54-atom supercells (numbers in square brackets). A negative charge corresponds to an extra electron charge, while negative displacements are directed towards the vacancy.

Sphere	Equilibrium atoms	V_U		V_N	
		d, Å	Δq, e	d, Å	Δq, e
(a)					
1	6	0.14[0.13]	0.03	−0.05[−0.03]	−0.23
2	12	−0.05	0.07	−0.01	−0.01
3	8	−0.03	−0.03	0.01	0
4	6	0.07	0.01	−0.10	−0.01

Sphere	Equilibrium atoms	Type	Hopping atom		Hopping atom	
			U		N	
			d, Å	Δq, e	d, Å	Δq, e
				0.09*		0.01*
(b)						
1	2	N/U	0.43 [0.40]	0.004	0.38 [0.39]	−0.09
2	4	U	0.05	0.09	−0.20	−0.03
2	4	N	−0.07/−0.11	−0.02	0.08	−0.12
3	4	U	0.10/0.13	0.13	0.01	−0.23
3	4	N	0.14	0.04	0.13/0.2	−0.07
4	8	U	−0.1	0.23	0.06	0.1
4	8	N	0.04	−0.04	−0.04	−0.05

* Charge change on interstitial ion.

In the *saddle point* of the vacancy migration process the hopping N or U ions have a different surrounding in the cube face position with only two pairs of NN ions of the opposite type. Despite the fact that the effective charges of the moving ions are close to those of host ions, the atomic displacements and charge redistribution essentially differ. As it follows from Table 1, the U or N ion at the saddle point considerably expands the surrounding lattice (atomic displacements ~0.4 Å, which are much larger than those in the equilibrium) whereas the charge redistribution is spread over four nearest neighbour spheres, especially for the U ion.

In order to simulate the realistic situation at high temperatures, a *double charged* U vacancy has been simulated using a special option in the VASP code with a compensating background charge homogeneously spread over the supercell. It turns out that the two holes added into the supercell (as compared to the neutral U vacancy) turn out to be almost randomly distributed over the supercell, probably due to the metallic nature of UN [8].

3.2. The effect of a substitutional O impurity

In a previous study [10] the O impurity has been modelled either as a substitution for a host N ion or in the interstitial position. It was found that in the former case the oxygen impurity does not produce lattice deformation but has an effective charge (of −1.37 e) that is slightly smaller than the charge of a host N ion (−1.66 e). It was also found that incorporation of oxygen into the UN lattice is energetically favourable, which explains effective UN fuel oxidation.

In the present paper a different situation is considered. The O impurity is in an equilibrium position and a N vacancy is present. When an O atom substitutes the host N ion in the 2nd NN position of the N vacancy, its local symmetry is reduced and six NN U ions split now into 3 groups of 2 ions each (Table 2). Their displacements vary from 0.025 to 0.049 Å. Some ions have a slightly smaller and others have a larger displacement than those around a single N vacancy (0.03 Å). Their excessive charges (compared to the perfect bulk charges) are very close, 0.30 e, and is similar to 0.22 e in the case of a single N vacancy. The effective charge of the O ion is −1.36 e, which is again close to that for a single substitutional defect. It is very slightly shifted towards the V_N.

Table 2
The effect of a substitutional O impurity on atomic displacements d (in Å) and effective charges q, (in e) near the N vacancy.

Type of NN ion	d, Å		q, e	
	U	O	U	O
Equilibrium	0.025(2x)	−0.01	1.36	−1.36
	0.049(2x)		1.38	
	0.032(2x)		1.37	
Saddle point	0.40	−0.07	1.24	−1.34
	0.45		1.51	

In a second step it was assessed how the substitutional O atom affects the atomic structure around the N vacancy in the saddle point position, being its next nearest neighbour. In the saddle point configuration of the N ion moving to the vacancy along the [1 1 0] direction, the two nearest U ions become non-equivalent as one is displaced by 0.40 Å whereas the other moves by 0.45 Å (compared with 0.40 Å for similar U ions at the saddle point of a single V_N). Their charges also differ. The effective charge of the O ion changes only slightly, and it is stronger displaced towards the V_N. The effect of the O impurity on the V_N migration energy is discussed in Section 4.

3.3. Different diffusion paths for interstitial N atoms

As revealed recently [9,16] (see also [17]), there are two possible mechanisms for the interstitial N ion migration: either direct jumps along the (0 0 1) axis (between positions I and II in Fig. 1) or the so-called *collinear interstitialcy mechanism* corresponding to the formation of the dumbbell at the saddle point (position III). Such a *dumbbell* is centered at a regular N site and could be oriented either along the [1 1 0] or the [1 1 1] direction (see more in Ref. [16]). In this paper, careful structure optimizations for the two dumbbells are performed. The basic results for the two migration paths are presented in Table 3.

The dumbbell formation leads to a considerable ($\geqslant$0.1 Å) lattice expansion up to the fourth ionic sphere. Furthermore, the (1 1 0) dumbbell is lower in energy than the (1 1 1) dumbbell. The dumbbell rotation from the (1 1 1) orientation to the (1 1 0) orientation requires only 0.37 eV.

On the other hand, the (1 1 1)-dumbbell bond breaking with formation of an interstitial N ion in a cube center (position I in Fig. 1) costs 1.74 eV. The effective charges of the two N atoms within the dumbbell are close to −1 e, which mimics the peroxy-radical $N_2^{(2-)}$. In this case, the electronic density of a host N ion is shared by two equivalent N ions (N_1, N_2) constituting a dumbbell, whereas the effective charges of four spheres of nearest neighbours are only slightly perturbed.

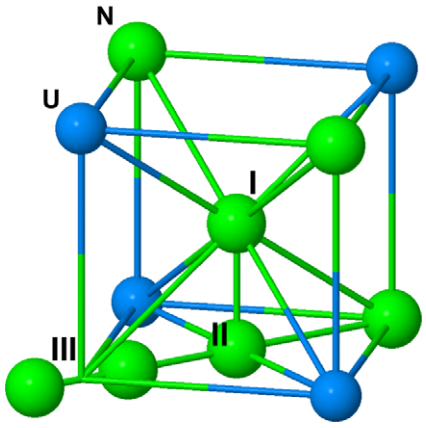

Fig. 1. Schematic view of the N ion at an interstitial position in a cube center (I) and the two possible mechanisms of its diffusion with the saddle points (II) and (III).

Table 3
The calculated relative total energies ΔE (in eV) (a), as well as the atomic displacements d (in Å) and the effective atomic charges q (in e) (b) for the two mechanisms of the interstitial N migration (illustrated in Fig. 1).

Position					ΔE, eV
(a)					
Cube center					0
(0 0 1) Jump					2.73
Dumbbells					
(1 1 0) d = 1.36 Å					1.37
(1 1 1) d = 1.41 Å					1.74
Sphere	Type	d, Å		q, e	
		[1 1 0]	[1 1 1]	[1 1 0]	[1 1 1]
(b)					
1	U	0.216	0.147	1.652	1.686
1	U	0.216	0.146	1.653	1.682
1	U	0.056	0.146	1.727	1.682
2	N	0.020	0.057	−1.658	−1.642
2	N	0.018	0.056	−1.658	−1.643
2	N	0.067	0.056	−1.620	−1.643
2	N	0.012	0.004	−1.618	−1.624
2	N	0.012	0.004	−1.618	−1.624
2	N	0.020	0.004	−1.634	−1.624
2	N	0.019	0.005	−1.634	−1.633
2	N	0.020	0.004	−1.634	−1.624
2	N	0.019	0.005	−1.634	−1.633
3	U	0.033	0.016	1.657	1.632
3	U	0.033	0.007	1.650	1.657
3	U	0.015	0.007	1.655	1.657
3	U	0.019	0.008	1.658	1.663
4	N	0.192	0.127	−1.629	−1.638
4	N	0.192	0.133	−1.634	−1.644
4	N	0.006	0.133	−1.629	−1.644
Dumbbell					
	N_1			−0.99	−1.04
	N_2			−0.98	−1.02
$N_1 + N_2$				−1.97	−2.06

This charge distribution is confirmed by the electron difference maps (Fig. 2) in the [1 1 0] dumbbell equilibrium position (Fig. 1). These figures demonstrate the local nature of the charge redistribution and reveal that the effective charges of the two N ions within the dumbbell fall between a neutral atom and a host ion (−1.66 e). One can also notice negligible interaction between the defects in neighbouring supercells.

It is interesting to compare these results with those for ionic MgO with the same *fcc.* structure. In MgO the energy required for the direct (0 0 1) jump is 2.12 eV, whereas for the collinearcy mechanism it is considerably smaller, i.e. 1.45 eV [16,18]. Lastly, migration via the (1 1 0) dumbbell in MgO has the lowest energy barrier too, by 0.15 eV smaller than via the (1 1 1) dumbbell. These findings are surprisingly similar to what is obtained here for UN, despite the different nature of the chemical bonding (but with similar crystalline structure).

3.4. Migration of interstitial U atoms

In the previous study [8] the formation energy for the N-type Frenkel pair within a 128-atom supercell was estimated to be 4.6 eV, where the lattice relaxation energy was 2.3 eV. In the present work corresponding values for the U-type Frenkel pair are obtained. Its formation energy turns out to be much larger, 9.92 eV, associated with the relaxation energy of 4.15 eV, both about twice larger than that for the N pair.

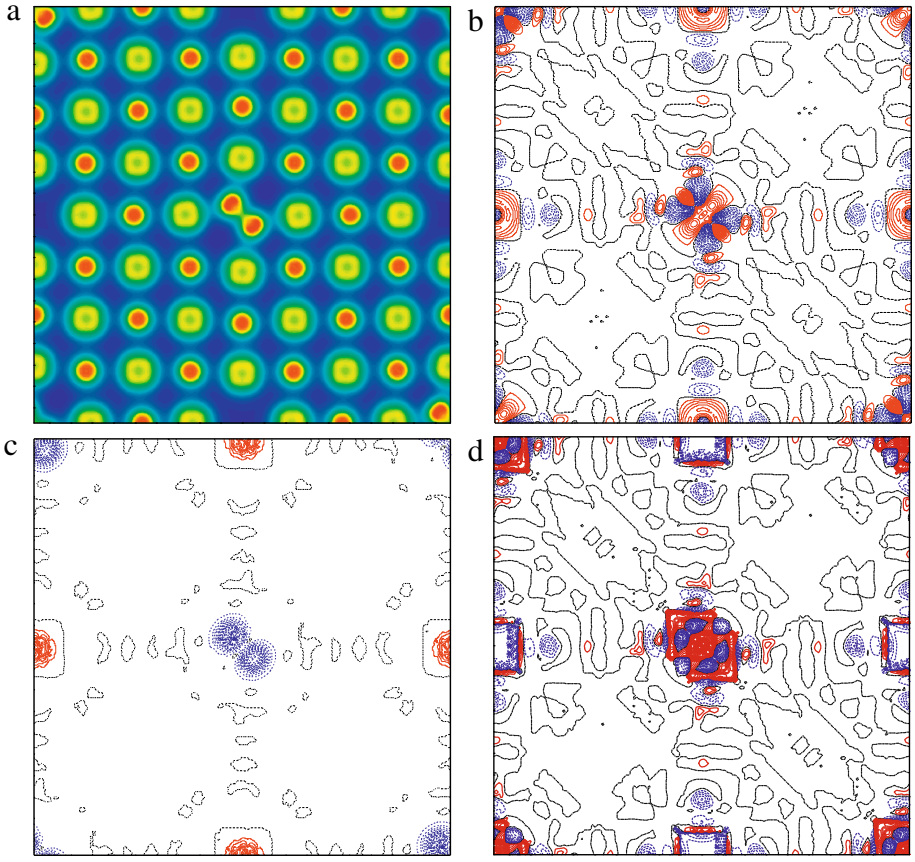

Fig. 2. A (1 1 0) cross-section of (a) the total and (b, c and d) the difference electron density of the interstitial dumbbell (Fig. 1). Plots (b), (c) and (d) are drawn with respect to the N_2 neutral molecule, a pair of neutral N atoms and N ions, respectively. Solid (red color) and dashed (blue color) lines correspond to deficiency and excess of electron density, respectively. The dash–dotted line (black in color) corresponds to a zero level. The density increments are 0.01 e /Å3 and 0.0112 e/Å3. (For interpretation of the references to color in this figure legend, the reader is referred to the web version of this article.)

The atomic relaxation and charge redistribution around the interstitial U ion in the equilibrium and saddle point position are summarized in Table 4. As one can see, even in the equilibrium position the interstitial U atom produces a considerable lattice expansion (~0.3 Å for the NN ions), which spreads up to the 4th NN. Its effective charge is close to + 0.85 e, mostly at the expense of the NN ions' charge redistribution. The saddle point is characterized by a large lattice expansion (0.6–0.7 Å) as well as a large charge redistribution (see Fig. 3).

The calculated ionic displacements around a V_U within the studied Frenkel pair in both the equilibrium and the saddle point configurations are similar to those for a single vacancy (Table 1).

3.5. GGA + U calculations

The DFT calculations described above were performed using the standard GGA exchange- correlation functional. This may give systematic errors due to an underestimation of the strong on-site Coulomb repulsion of the 5*f* electrons in actinides, and a consequent failure to capture the correlation-driven localization. In order to take these effects into account, the so-called GGA + *U* approach (in which the semi-empirical on-site correlation parameter *U* needs to be fitted to reproduce a certain set of experimental data such as band gaps, structural properties, or magnetic moments) could be used [19–21]. However, there is an ongoing debate about

Table 4
The atomic displacements *d* (in Å) and charge redistribution Δ*q* (in e) for a U interstitial at the equilibrium position (cube centre) and at the saddle point (face center) with respect to the corresponding defect-free supercell. Numbers with/show dispersion in properties for ions in the same sphere.

Cube centre					Face centre			
Sphere	Equivalent atoms	Type	*d*, Å	Δ*q*, e −0.97*	Equivalent atoms	Type	*d*, Å	Δ*q*, e −1.51*
1	4	U	0.36	0.64	2	U	0.69	−0.85
1	4	N	0.27	0.30	2	N	0.60	0.33
2	12	U	0.04	−0.03	4	U	−0.05	−0.23
2	12	N	0.10/0.13	0.11	4	N	0.16	0.25
3	12	U	0.06	−0.24	4	U	±0.01/0.15	−0.04/0.02
3	12	N	0.01	0.03	4	N	0.29	0.13/0.21
4	13	U	0.01/0.08	−0.03	8	U	0.08	−0.17
4	13	N	±0.04/0.12	0.07/0.31	8	N	−0.03	0.08

* Change of interstitial U atom charge.

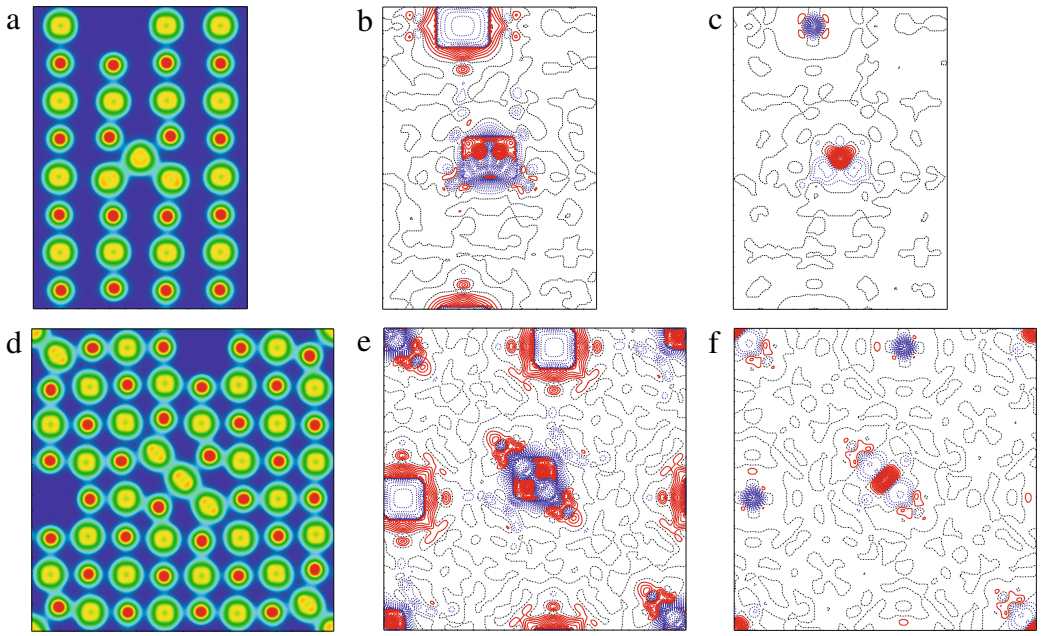

Fig. 3. The total (a and d) and the difference (b, c, e and f) electronic density maps for the interstitial U ion at the equilibrium position (a, b, c: at the cube center, cross section along the [1 0 0]) plane and at the saddle point (d, e, f: at the face center, cross section along the [1 1 0] plane), respectively, for a U ion (b and e) and a neutral U atom (c and f). Solid (red color) and dashed (blue color), lines correspond to deficiency and excess of electron density, respectively. Dash–dotted lines (black color) designate a zero level (density increments are 0.01 e/Å3 and 0.0112 e/Å3). (For interpretation of the references to color in this figure legend, the reader is referred to the web version of this article.)

the application of this approach to systems containing (point- or spatially-extended) defects because they violate the solid-state periodicity and create non-equivalency between formerly equivalent atoms. In a periodic system (such as a defect-free, antiferromagnetic UN crystal), one can calibrate the parameter *U* in the GGA + *U* method in such a way that the experimental value of the U magnetic moment is reproduced [22] (however, an exact value of the lattice constant may correspond to a different *U* value). It is, however, unclear whether one can describe the Coulomb repulsion and localization effects on non-equivalent *f*-metal atoms (e.g. on atoms with different coordination) surrounding the defect site using just a single value of the parameter *U*. It has already been discussed whether the parameter *U* depends on the local structure and the defect surrounding. In particular, one should be careful when using the same *U* for fitting the lattice constant (or the band gap) in PuO_2 and Pu_2O_3 [23] or in CeO_2 and Ce_2O_3 [24]. Another problem of the GGA + U approach is the presence of metastable electronic states and the necessity to find the real ground state (more details in Ref. [23]). So far, only a few papers were published with a discussion of applying the GGA + *U* approach to a system with defects.

In the present paper, the GGA + *U* calculations were used for the migration of interstitial N atom using the same VASP 4.6 code [12], together with the PAW relativistic pseudopotentials, and the plane-wave basis. More precisely, the simplified (rotationally invariant) approach to the GGA + U, derived by Dudarev et al. [25], was employed. In this approach the parameters U and J (corresponding to the exchange interaction) do not enter separately, and only the difference (U-J) is meaningful. The value for the difference ~ 2 eV reproduces the correct value for the magnetic moment at the uranium atoms for the periodic, antiferromagnetic UN crystal [22] when combined with the spin–orbit coupling effects. First, a poor convergence of the results was noticed. Second, it was observed that using two different methods of matrix diagonalization (the Davidson block iteration scheme and the residual minimization method) different values of the converged total energies were obtained (which differ by $\sim$1 eV for the same set of the *k*-points), which was never observed for the GGA functionals. Third, the energy barrier for a direct (0 0 1) jump of a nitrogen atom from the interstitial cube center obtained from the Davidson scheme is only 0.29 eV, which seems to be unrealistically small.

It is still unclear why the GGA + U approach fails for defects in UN. Nevertheless the standard GGA calculations without U reproduce well basic crystal properties [7,8] (except for the low-temperature magnetic properties [1,22]) and give the correct UN metal-type behaviour (i.e., a zero band gap). This is radically different from the case of uranium dioxide (UO_2) where the GGA calculations converge to a metal-type electronic structure (instead of the experimentally observed semiconductor type structure), and the gap does not open with a zero value of the parameter *U* [26]. In the case of UN the standard GGA approach seems therefore to be sufficient for defect studies with large formation and migration energies.

4. Migration energies

The *defect migration* energies were calculated in the standard way, as the difference of the total energy for defects in their equilibrium and saddle point configurations after relaxation. The summary is presented in Table 5.

The migration energies of N and U vacancies calculated using the 54-atom supercells are very close, $\sim$3.5 eV. These results were verified using the 250-atom supercell containing two well separated dissimilar vacancies moved independently to the interstitial position. The migration energies obtained are slightly smaller (probably, due to the reduced interaction between periodically distributed defects and the difference in supercell stoichiometry) but again very similar, 3.2–3.3 eV. This contrasts with results for defects in UO_2 where the U vacancy is known to be much less mobile than the oxygen vacancy (with migrations energies of 3.4 and 0.5 eV, respectively) [1]. This discrepancy could arise from a considerable difference in crystalline structures (rock-salt vs fluorite). On the other hand, the same trend is observed for the interstitial U

Table 5
Summary of the calculated migration energies (eV).

N vacancy	
Single defects	3.50 (3.3)[a]
O impurity as 2nd NN	2.84
U vacancy	3.52[b] (3.15)[a]
N interstitial	
Along the (0 0 1)	2.73
(1 1 0) dumbbell	1.37
(1 1 1) dumbbell	1.74
U interstitial	0.65
O interstitial impurity along (0 0 1) [9,10]	2.85

[a] 250-atom supercell.
[b] 3.49 eV for double charged defect.

and N as in the UO_2 (0.4 and 0.8–1.0 eV, respectively [1]). The trend in Frenkel pair formation energies is also similar to that obtained for the UO_2: the energy for the U pair is about twice that for the anion (N or O) pair. The calculations also indicate that a substitutional O impurity can considerably reduce the migration energy of the N and U vacancies.

The migration energy of the host interstitial N ion along the [0 0 1] direction is smaller (2.73 eV) than that for the N vacancy, and is close to the migration energy of the O impurity. This is reasonable, since both ions have a comparable size and charge. However, the energetically most favourable N ion migration is predicted to occur via the *collinear interstitialcy* mechanism, with an activation energy of only 1.74 eV. The three- dimensional diffusion of an interstitial N ion can occur via a combination of the dumbbell rotations (with the energy cost of 0.37 eV) and the rate-determining (1 1 1) jumps. This mechanism is well known in ionic solids with the same fcc. structure [16–18], such as alkali halides and oxides. Our results could point at a *universal mechanism* of the interstitial ion migration in fcc. solids with very different chemical nature. The migration energy of the interstitial U ion (0.65 eV) is surprisingly small, probably due to the smaller U^{3+} effective radius (~1 Å) as compared to the N^{3-} ion (1.46 Å) [27]. Using the mass action law [1] the Arrhenius diffusion energy for U interstitials is estimated to be 5.6 eV.

5. Implementing the first principle results in the fuel performance prediction

For designing nuclear fuels or assessing their life-time in a reactor, systematic recourse is made to fuel performance codes that account for various macroscopic aspects of the fuel behaviour including its thermal and mechanical performance as well as the evolution of the fissile isotopes under the influence of varying neutron fluxes, temperature gradients and thermodynamic forces. One such tool is the TRANSURANUS code, developed in the 1970s for FBR fuels and containing material properties for various actinide fuels such as mixed carbides, nitrides and oxide fuels [28]. The design of advanced nuclear fuels for Generation-IV reactors, however, requires an update of some material properties and models based on experimental data available in the literature. Unfortunately, not all parameters involved in the macroscopic fuel performance codes are directly accessible through experiments. Thanks to the development of more sophisticated simulation tools like the DFT method, one can estimate some of those parameters and assess the impact of fabrication imperfections such as impurities. This can shed light on the basic mechanisms, and contribute to limit the amount of expensive and time-consuming experiments.

The example considered here is the Arrhenius activation energy for thermal creep in UN fuel, as very little data are available in the open literature. Fuel creep is generally modelled as a sum of primary (or transient) and secondary (or stationary) creep. The stationary creep component, in turn, can be dominated by irradiation-induced creep at low temperatures (typically below 1300 K) or by thermally activated creep mechanisms such as Nabarro–Herring creep (vacancy diffusion) or dislocation climb. The correlations for thermal creep adopted in nuclear fuel performance codes are therefore characterized by an Arrhenius activation energy, consisting of the formation plus migration energy for the moving defect under consideration. The formation energy is taken as half the Frenkel defect formation energy, being 2.3 and 5 eV for anions and cations in UN respectively (cf. Section 3.4). Based on the migration energies listed in Table 5, the Arrhenius activation energies for the U and N vacancies are therefore E_{Uv} = 8.5 eV and E_{Nv} = 5.8 eV (E_{Nvo} = 5.14 eV when an O impurity is nearby), respectively. Similarly, for the U and N interstitials, one obtains an Arrhenius activation energies of E_{Ui} = 5.6 eV and E_{Ni} = 3.67 eV (for the dumbbell mechanism), respectively. The U vacancy is therefore expected to be the slowest moving species in UN.

Philibert [11] analysed the relation between creep and diffusion for fast breeder oxide and carbide fuels. It was concluded that the creep rate is proportional to some diffusion coefficient, whatever the exact nature of the deformation mechanism: Nabarro viscuous creep, recovery creep or pure climb creep. It was explained that this diffusion coefficient is an effective diffusivity, which is often (but not always) dominated by the slowest moving species. Finally it was underlined that activation energies for creep rate and for diffusion of the slowest species agree only with a rather large uncertainty, like in metals.

The experimental stationary creep rates reported by Uchida and Ichikawa [4] were obtained for UN fuel with 91% of the theoretical density and temperatures between 1573 and 1773 K. More recently, Hayes et al. [3] provided a correlation for the secondary creep rate (s^{-1}) on the basis of another set of experimental data:

$$\dot{\varepsilon} = f(P) \times 2.05410^{-3} \times \sigma^{4.5} \times \exp\left(-\frac{39369.5}{T}\right), \quad (1)$$

where the stress σ is expressed in MPa, T represents the temperature (K) and $f(P)$ is a function of the porosity (P):

$$f(P) = \frac{0.987}{(1-P)^{27.6}} \exp(-8.65P). \quad (2)$$

The experimental data used by Hayes [3] were obtained from UN fuel with an oxygen impurity of 400 ppm. Their correlation is plotted in Fig. 4, together with the experimental data from Uchida and Ichikawa [4] obtained from UN fuel with 3000 ppm oxygen.

Fig. 4 reveals that the activation energy of UN samples with higher oxygen content is smaller, which is in qualitative agreement with the VASP computations presented above. Furthermore, the activation energy in the correlation of Hayes et al. corresponds to 3.4 eV and is in good quantitative agreement with the activation energy computed by means of the VASP code for the N interstitials migrating via the (1 1 0) dumbbell: E_{Ni} = 3.67 eV. This might be interpreted as if the thermal creep in UN is dominated by interstitial diffusion alone. Nevertheless, there appears to be a large scatter in the experimental data for the Arrhenius activation energy of thermal creep in UN. The Arrhenius activation energy of 5.5 eV applied in the thermal creep (s^{-1}) correlation in the TRANSURANUS code:

$$\dot{\varepsilon}_{th} = 14.9 \times 10^{+9} \times \sigma^{2.44} \times \exp\left(-\frac{63200}{T}\right), \quad (3)$$

agrees relatively well to the bulk of data compiled by Matzke [1,29], which corresponds to the Arrhenius activation energy for a migrating N vacancy or a U interstitial. However, Matzke et al. have also reported an activation energy of 3.2 eV in a temperature range of 1573 to 1873 K. Furthermore, it must be underlined that the Arrhenius activation energy applied in the fuel performance code does

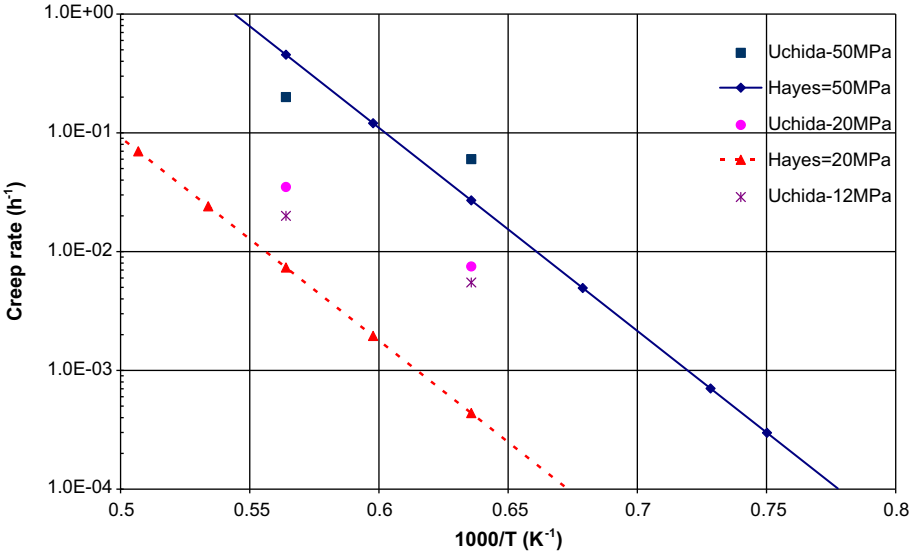

Fig. 4. Thermal creep rate for UN fuel according to the correlation of Hayes et al. [3] and compared with experimental data reported by Uchida and Ichikawa [4].

not correspond to a single creep mechanism or migrating species. Instead, the correlation considers two stationary creep components; one irradiation-induced creep component that depends on the local neutron flux density and stress, plus one thermally activated component that depends on the local stress and temperature. The second term represents a combination of different basic creep processes, and cannot be unambiguously associated with a single mechanism such as Nabarro–Herring creep (based on vacancy diffusion). It is therefore fair to conclude that there is a quantitative agreement between the Arrhenius activation energies for diffusion obtained by means of the first principle calculations of VASP (between 3.67 and 8.5 eV) and the experimental data for creep (between 3.2 and 5.5 eV) when taking into account the uncertainties. This is in line with the conclusions of Philibert [11] for oxides and carbides.

In order to analyse the impact of the oxygen on the thermal fuel creep under FBR conditions, the simulation of a typical nitride fuel pin in the JOYO reactor was carried out by means of the TRANSURANUS code, based on the parameters reported by Tanaka et al. [30]. The evolution of the linear heat rate is shown at three axial levels of the fuel rod in Fig. 5.

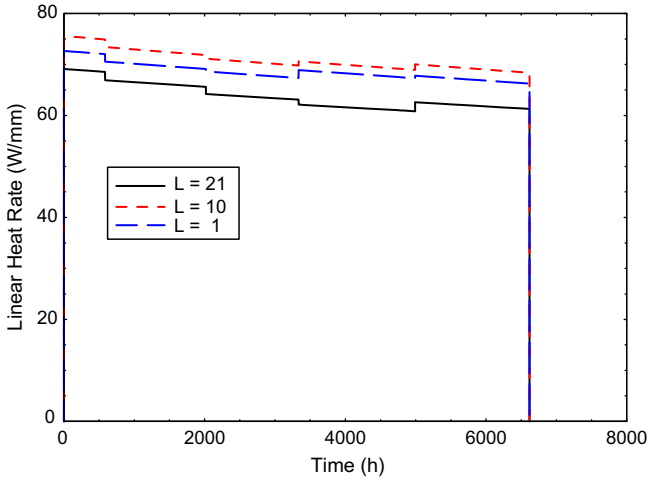

Fig. 5. The linear heat rate of a representative fuel rod irradiated in the JOYO reactor [30] at three different levels in the fuel rod: at the bottom ($L = 1$) and top of the fuel pin ($L = 21$), as well as at the middle axial position ($L = 10$).

The effect of oxygen impurities on the mechanical performance of the nitride fuel via the impact on the thermal creep component is shown in Fig. 6. The oxygen promotes thermal creep by reducing the activation energy, resulting in a very modest increase of the radial expansion (~1 μm) and a decrease of the axial expansion of the fuel column (0.1 mm) in the case under consideration.

The modest effect of the oxygen impurity on the axial expansion as a result of the thermal creep component is due to the moderate temperature levels obtained in nitride fuels under normal operation conditions in a FBR reactor. The predicted central temperatures in the upper part of the fuel pin are shown in Fig. 7 for three different activation energies for thermal creep. The figure reveals that the central temperature remains modest in comparison with those expected for mixed oxide fuel under the same conditions thanks to a better thermal conductivity of the nitride fuel. As a consequence, the considered variations of the activation energies of the thermal creep have only a minor influence on the fuel temperature in this example.

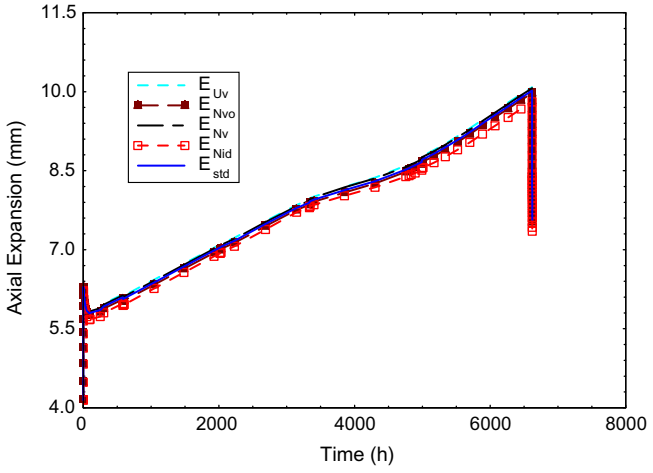

Fig. 6. Simulation of the fuel axial expansion in a typical UN fuel rod irradiated in the JOYO reactor [30] by means of the TRANSURANUS code, to illustrate the effect of oxygen on thermal creep. The standard activation energy (E_{std}) applied in the TRANSURANUS code is 5.5 eV, whereas E_{Nid} (= 3.67 eV), E_{Uv} (= 8.5 eV), E_{Nv} (= 5.8 eV) and E_{Nvo} (= 5.14 eV) are inferred from Table 5.

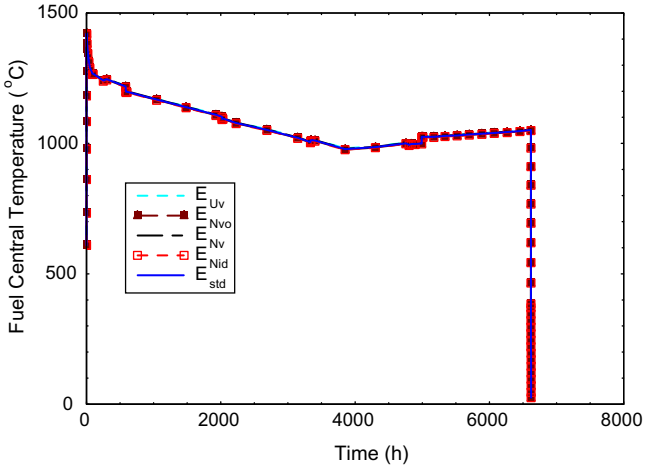

Fig. 7. Central temperature evolution prediction by means of the TRANSURANUS code in a representative nitride fuel rod irradiated in the JOYO reactor. The standard activation energy (E_{std}) applied in the TRANSURANUS code is 5.5 eV, whereas E_{Nid} (= 3.67 eV), E_{Uv} (= 8.5 eV), E_{Nv} (= 5.8 eV) and E_{Nvo} (= 5.14 eV) are inferred from Table 5.

6. Conclusions

First principles calculations by means of the VASP code have been applied to predict realistic defects properties in advanced actinide materials, in particular nuclear fuels. Such computer simulations are much faster and cheaper than the relevant experiments. It was observed that the formation energy of the U-type Frenkel pair exceeds nearly twice that for the N-type pair. On the other hand, the Schottky formation energy is close to that for an N-type Frenkel. This is why intrinsic N interstitials and vacancies could exist in comparable concentrations and both contribute to the defect transport. Similar migration energies for U and N vacancies in UN are also predicted; hence the same effect can be expected in UC that has a similar fcc. structure.

Based on the first principle predictions, the analysis of thermal creep in UN was performed, which showed that the VASP calculations are in qualitative agreement with the effect of oxygen on the reduction of the activation energy for thermal creep reported in the literature, as well as in quantitative agreement with the experimental data when taking into account the uncertainties. The implementation in the TRANSURANUS fuel performance code illustrates how first principle calculations can contribute directly to a multi-scale approach that is being developed for designing advanced nuclear fuels.

The next steps for improving the TRANSURANUS fuel performance predictions for nitride fuel include the implementation of improved values for the specific heat obtained by means of first principle calculations and the development of specific models for the fuel relocation as well as the fission gas release and swelling in UN fuel.

Acknowledgments

This study was partly supported by the Latvian National Programme on Energetics, the European Union FP7 F-BRIDGE project (Contract No. 211690), the Idaho National Laboratory (INL) Directed Research and Development program, and the US Department of Energy, Office of Nuclear Energy under DOE Idaho Operations Office, Contract No. DE-AC07-051D14517. This research used resources of the National Energy Research Scientific Computing Center (NERSC), which is supported by the Office of Science of the US Department of Energy under Contract No. DE-AC02-05CH11231 and the EMS Laboratory of the PNNL (Project No. 25592). It was also supported in part by a grant of computer time from High Performance Computer Center at INL. Authors are also greatly indebted Hj. Matzke, R.A. Evarestov, V.V. Rondinella, E. Heifets, D. Gryaznov, and R. Caciuffo for many stimulating discussions.

References

[1] Hj. Matzke, Science of Advanced LMFBR Fuels, North Holland, Amsterdam, 1986.
[2] R. Agarwal, V. Venugopal, D.D. Sood, J. Nucl. Mater. 270 (1999) 301.
[3] S.L. Hayes, L.K. Thomas, K.L. Peddicord, J. Nucl. Mater. 171 (1990) 271.
[4] M. Uchida, M. Ichikawa, J. Nucl. Mater. 49 (1973) 91.
[5] K. Kurosaki, K. Yano, K. Yamada, M. Uno, S. Yamanaka, J. Alloy Compd. 313 (2000) 242.
[6] R.A. Evarestov, A.V. Bandura, M.V. Losev, E.A. Losev, E.A. Kotomin, Yu.F. Zhukovskii, D. Bocharov, J. Comput. Chem. 29 (2008) 2079.
[7] R. Atta-Fynn, A.K. Ray, Phys. Rev. B 76 (2007) 115101.
[8] (a) E.A. Kotomin, R.W. Grimes, Yu. Mastrikov, N.J. Ashley, J. Phys.: Condens. Matter 19 (2007) 106208;
(b) E.A. Kotomin, Yu.A. Mastrikov, Yu.F. Zhukovskii, P. Van Uffelen, V.V. Rondinella, Phys. Status Solidi C4 (2007) 1193.
[9] E.A. Kotomin, D. Gryaznov, R.W. Grimes, et al., Nucl. Inst. Meth. B 266 (2008) 2671.
[10] E.A. Kotomin, Yu. Mastrikov, J. Nucl. Mater. 377 (2008) 492.
[11] J. Philibert, Solid State Ionics 12 (1984) 321.
[12] G. Kresse, J. Hafner, VASP the Guide, University of Vienna, 2003.
[13] J.P. Perdew, Y. Wang, Phys. Rev. B 45 (1992) 13244.
[14] G. Henkelman, A. Arnaldsson, H. Jónsson, Comput. Mater. Sci. 36 (2006) 254.
[15] H.J. Monkhorst, J.D. Pack, Phys. Rev. B 13 (1976) 5188.
[16] E.A. Kotomin, A.I. Popov, Nucl. Inst. Meth. B 141 (1998) 1.
[17] K. Govers, S. Lemehov, M. Hou, M. Verwerft, J. Nucl. Mater. 366 (2007) 161.
[18] T. Brudevoll, E.A. Kotomin, N.E. Christensen, Phys. Rev. B 53 (1996) 7731.
[19] V.I. Anisimov, J. Zaanen, O.K. Andersen, Phys. Rev. B 44 (1991) 943.
[20] A.I. Liechtenstein, V.I. Anisimov, J. Zaanen, Phys. Rev. B 52 (1995) R5467.
[21] V.I. Anisimov, F. Aryasetiawan, A.I. Liechtenstein, J. Phys.: Condens. Matter 9 (1997) 767.
[22] D. Gryaznov, E. Heifets, E.A. Kotomin, Phys. Chem. Chem. Phys. (2009), doi:10.1039/b907233k.
[23] G. Jomard, B. Amadon, F. Bottin, M. Torrent, Phys. Rev. B 78 (2008) 075125.
[24] C.W.M. Castleton, J. Kullgren, K. Hermansson, J. Chem. Phys. 127 (2007) 244704.
[25] S.L. Dudarev, G.A. Botton, S.Y. Savrasov, C.J. Humphreys, A.P. Sutton, Phys. Rev. B 57 (1998) 1505.
[26] M. Iwasawa, Y. Chen, Y. Kaneda, M. Kinoshita, Mater. Trans. 47 (2006) 2651.
[27] C. Giacovazzo, Fundamentals of Crystallography, Oxford University Press, 2002. p. 420.
[28] K. Lassmann, J. Nucl. Mater. 188 (1992) 295.
[29] IAEA-TECDOC-1374, Development status of metallic, dispersion and non-oxide advanced and alternative fuels for power and research reactors, September 2003, IAEA, ISBN: 92-0-110303-4, ISSN: 1011-4289.
[30] K. Tanaka, K. Maeda, K. Katsuyama, M. Inoue, T. Iwai, Y. Arai, J. Nucl. Mater. 327 (2004) 77.